Special Perforated Steel Plate Shear Walls with Reduced Beam Section Anchor Beams. II: Analysis and Design Recommendations

Darren Vian, M.ASCE[1]; Michel Bruneau, M.ASCE[2]; and Ronny Purba[3]

Abstract: This paper presents a comparison of analytical and experimental results from an investigation of specially detailed ductile perforated steel plate shear walls (SPSWs). These SPSWs had low yield strength steel infill panels, anchor beams with reduced beam sections connections, and were specially detailed to accommodate utility passage through the wall while remaining ductile. Finite-element models of full SPSWs and subelement strips are developed using the finite element software package ABAQUS/Standard to facilitate a comparison with experimental results and to investigate the influence of localized distribution of panel stress and strain between perforations. Based on the analytical and experimental results, recommendations for the design of these special detailed perforated SPSWs are presented.

DOI: 10.1061/(ASCE)0733-9445(2009)135:3(221)

CE Database subject headings: Shear walls; Steel plates; Earthquake engineering; Beams; Seismic design.

Introduction

Steel plate shear walls are a single or multistory lateral force resisting system consisting of thin, unstiffened, infill plates connected to their boundary frames. Upon lateral loading, buckling occurs in the infill plates, precipitating the development of a tension field action that resists the applied lateral forces.

A recent experimental investigation of single-story, single-bay steel plate shear wall (SPSW) frames was conducted to investigate the behavior of specially detailed ductile perforated SPSWs designed to accommodate utility passage and having anchor beams with reduced beam sections (RBSs) connections [see companion paper (Vian et al. 2009)]. Two specimens were designed to accommodate utility passage, one having multiple holes specially laid out in the steel panel (P) and the other with quarter-circle corner cutouts (CR). An additional specimen was designed with a solid infill panel (S2) as a reference specimen. The specimen P also has reduced panel strength and stiffness compared to the corresponding SPSW having a solid panel. The results of the experimental program showed all specimens resisted a history of increasing cyclic displacement up to a minimum drift of 3% and that the perforated panel reduced the elastic stiffness and overall strength of the specimen by 22 and 15%, respectively, as compared with the solid panel specimen.

[1]Structural Engineer, Parsons Brinckerhoff, New York, NY 10119. E-mail: Vian@pbworld.com; formerly, Graduate Research Assistant, Dept. of CSEE, Univ. at Buffalo, Amherst, NY 14260.

[2]Professor, Dept. of CSEE, Univ. at Buffalo, Amherst, NY 14260. E-mail: bruneau@buffalo.edu

[3]Graduate Research Assistant, Dept. of CSEE, University at Buffalo, Amherst, NY 14260.

Note. Associate Editor: Benjamin W. Schafer. Discussion open until August 1, 2009. Separate discussions must be submitted for individual papers. The manuscript for this paper was submitted for review and possible publication on June 22, 2007; approved on November 5, 2008. This paper is part of the ***Journal of Structural Engineering***, Vol. 135, No. 3, March 1, 2009. ©ASCE, ISSN 0733-9445/2009/3-221–228/$25.00.

This paper presents the modeling and analysis of the experimental specimens using the finite-element (FE) method and the results of an analytical study of full and subelement SPSWs to investigate the influence of localized distribution of panel stress and strain between perforations. Finite-element models of the individual specimens and subelement (strips) were developed using the commercially available software package ABAQUS/Standard (HKS 2002). Observations, as well as design recommendations and considerations based on the results of the analytical and experimental investigation, are presented.

Finite-Element Modeling

Model Description

Finite-element models of the tested specimens were developed for comparison with experimental results and to further investigate the behavior of the frame members and the infill panel. Frame members were modeled explicitly as built-up sections of plate elements to capture local buckling and plastic hinging observed in the specimens during testing. The connection tab, or "fish plate," used in the experiments to connect the infill panel with the surrounding frame, was neglected in the finite element modeling. Instead, a direct connection was assumed to take place between the two structural elements, an approximation whose effects on analysis results were found to be negligible (Driver et al. 1997). Both the infill panel and boundary frame members were modeled using the four-noded S4R element, a general purpose shell with reduced integration (HKS 2002), to avoid shear locking. The hinge at the base of each specimen column was not modeled explicitly in the ABAQUS model. Instead, "CONN3D2" connector elements were used to connect a reference node at the location of the hinge center with nodes at the tip of each flange and the intersection of the flanges and web. All degrees of freedom (DOF) with the exception of rotation about the out-of-plane axis were restrained at the reference node located at the center of the hinge

to replicate the hinge rotation permitted during testing. The out-of-plane resistance provided by the lateral supports at the top of columns during the experiments was modeled by restraining displacements in that direction. The exterior nodes of the flange elements around the perimeter of the panel zones were restrained against movement in the z-direction (out of plane) to replicate conditions at the points of load application (as intended for the experiment, as detailed modeling of the lateral support frame was not expected to provide additional useful information with regard to the observed overall specimen behavior).

The initial shape of each specimen infill panel was not recorded prior to testing, although some small out-of-plane deformations (deviation from perfect flatness) were visually observed. These imperfections help precipitate the global panel buckling and, therefore, need to be considered in the FE analysis of the specimens. To account for the initial imperfections, an eigenvalue buckling analysis was performed to determine the first infill panel buckling mode prior to cyclic analysis of each specimen model. The first panel buckling mode multiplied by a small displacement amplitude (e.g., 1 mm) was applied as the initial conditions of the specimen P, CR, and S2 for cyclic analysis. The magnitude of the imperfections was not found to be significant, as buckling of the plate occurred as soon as the system drifted.

Although a number of nested surface models appear in the literature (Hodge 1957; Dafalias and Popov 1975; Krieg 1975), the nested surface model provided within ABAQUS/Standard and based on the work of Lemaitre and Chaboche (1990) (known as the "HARDENING=COMBINED" model in ABAQUS) was used to represent the stress-strain behavior of both the infill panel material (LYS165) and the frame member material (A572). This pressure and rate independent material model implements the concepts of both isotropic hardening (i.e., an expansion of the yield surface while undergoing plastic strains) and kinematic hardening (i.e., a shifting of the yield surface without expansion during plastic straining), overcoming inadequacies exhibited by using either of these hardening rules alone in modeling cyclic problems. The kinematic hardening component of the material model could be defined in multiple ways, depending on the type of test data available, using pairs of "true" stress (Cauchy stress) and logarithmic strain, σ_{true} and ε_{ln}, respectively. Since only standard monotonic tension tests (not cyclic) were performed on specimen material coupons, the specification of inelastic material properties for the analytical model required some assumptions. For the infill panel material, the available half-cycle test data were used to generate input for ABAQUS to define kinematic hardening. The boundary frame members were built-up sections, fabricated from plate material specified as ASTM A572 Gr. 50 (F_y =345 MPa). As with the infill panel material, only monotonic uniaxial tension tests were performed on material coupons. However, since the material was specified to conform with ASTM A572 and exhibited a nearly identical yield plateau stress, the cyclic behavior—for the purposes of the analysis—was assumed equivalent to that of "Steel A" documented in an ATLSS study of cyclic inelastic strain behavior on properties of A572 Gr. 50 steel (Kaufmann et al. 2001).

Load was applied to the FE models through a specified top beam displacement history consisting of a series of cyclic displacement curves with increasing amplitude. The amplitude of each displacement excursion was determined from the interstory displacement history recorded during testing of each specimen.

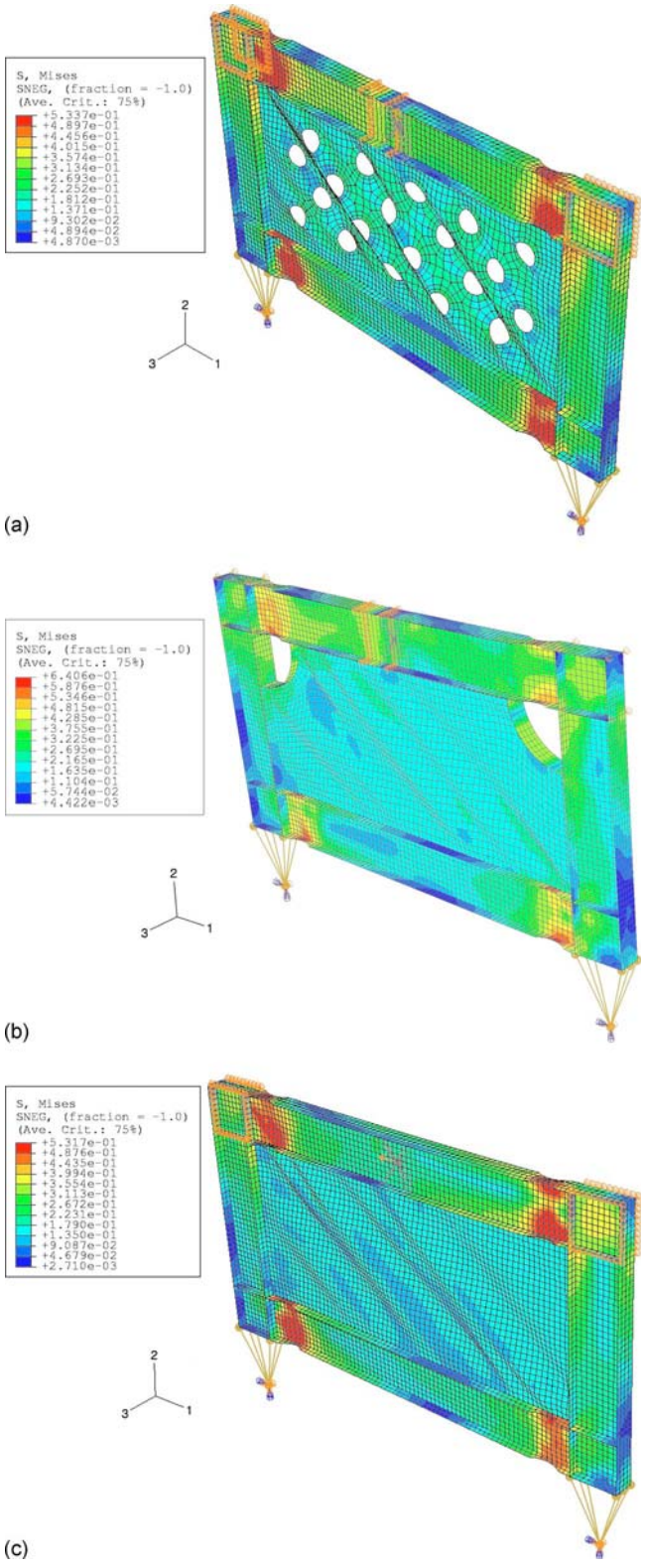

Fig. 1. Deformed shape of FE models at 3% drift: (a) P; (b) CR; and (c) S2

Comparison of Results

Fig. 1 shows the deformed shape of each model at a lateral displacement corresponding to 3% interstory drift, and contours representing the magnitude of the von Mises stress (in 10^{-3} MPa). Fig. 1(a) shows the FE model of specimen P. The stress concen-

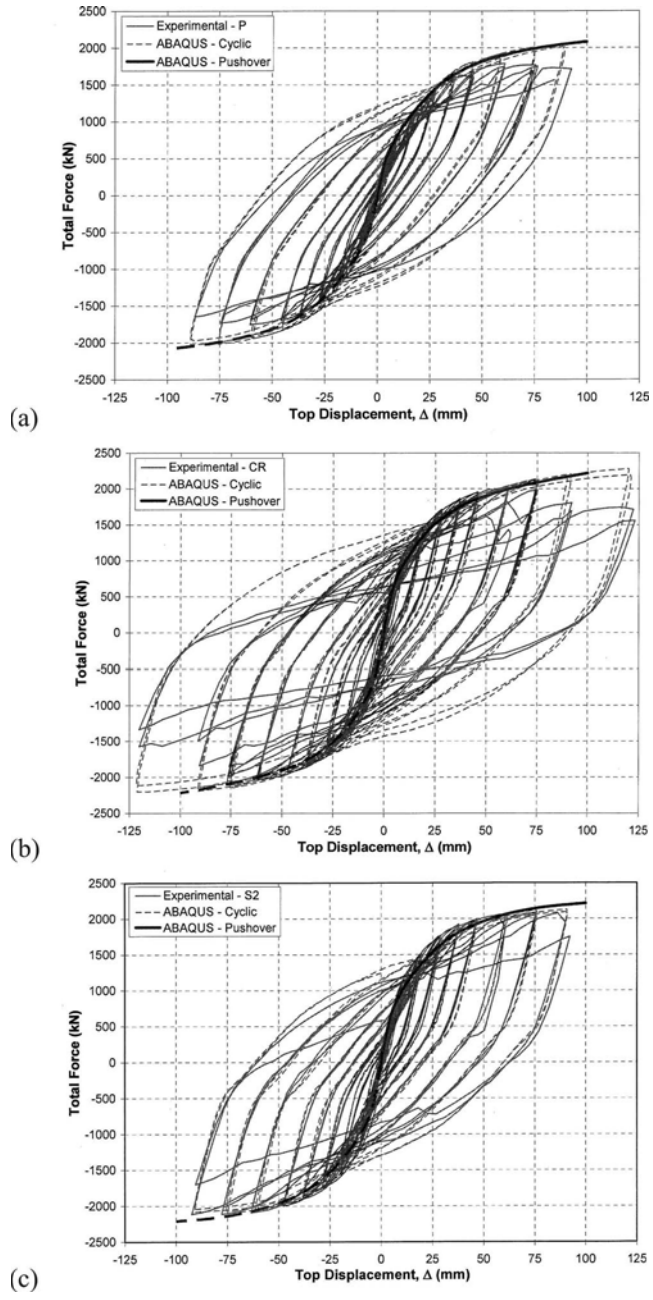

Fig. 2. Comparison of experimental and analytical results (a) P; (b) CR; and (c) S2

trations obtained at the RBS locations are consistent with those observed during testing (by flaking of white wash as a qualitative measure of yielding). Fig. 1(b) shows the FE model of specimen CR, again highlighting stress concentrations in the RBS. Fig. 1(c) shows the FE model of specimen S2 again with von Mises stress contours.

Presented in Fig. 2 is a comparison of the analytically predicted monotonic and cyclic results from the models of the P, CR, and S2 specimen with the experimentally obtained results. The monotonic pushover and cyclic results from ABAQUS analyses of the P specimen, together with the total force versus top beam displacement hysteresis obtained from experimental testing, are presented in Fig. 2(a). Though the analytical model slightly overestimates the experimental strength, good agreement between the experimental and cyclic analytical results is observed for cycles

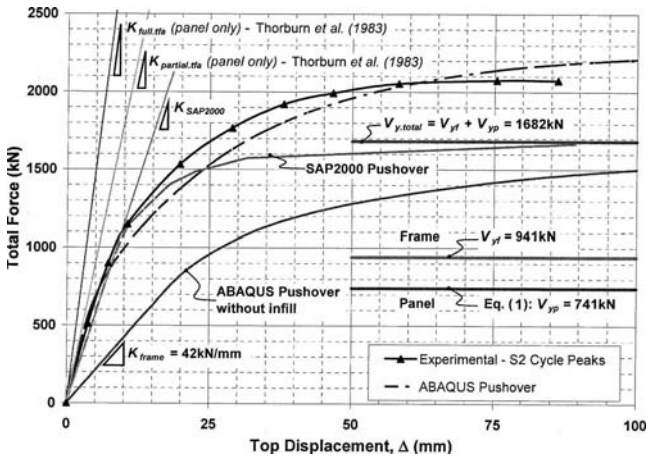

Fig. 3. Comparison of S2 backbone force–displacement curve with various analytical models

up through an approximate top displacement amplitude of 37 mm. During subsequent cycles beyond a 37 mm displacement amplitude, the loading assembly rotated followed by column twisting and distortion of the top beam and the lateral support frame as described in Vian et al. (2009). Since the lateral support frame was not explicitly modeled, the FE analysis did not capture the succession of distortions observed in the experiment and corresponding reduction in strength, but instead captured behavior closer to actual boundary conditions in a building.

Presented in Fig. 2(b) is a comparison of the monotonic and cyclic results from the FE model of specimen CR with the total force versus top beam displacement hysteresis from experimental testing. The initial stiffness of the analytical models (both pushover and cyclic) overestimated the experimentally determined stiffness; however, after the formation of tension field action, the predicted stiffness of the FE model reduced, improving the agreement between the analytical and experimental values. Good agreement between the predicted strength from the cyclic FE analysis and the experimental results are observed up to a displacement amplitude of 76 mm. During the subsequent cycle, the flanges in the bottom beam RBS connection ruptured decreasing the load the specimen could resist. The FE model did not account for material fatigue and, therefore, could not capture the reduction in strength for cycles of larger amplitude.

Presented in Fig. 2(c) is a comparison of the cyclic results from FE analysis of specimen S2 with the total force versus top beam displacement hysteresis obtained from experimental testing. Excellent agreement in hysteretic behavior is observed until the final cycle, during which fracture occurred in the bottom flange of each bottom beam RBS connection and the strength of the specimen dropped by approximately 20%.

Fig. 3 presents monotonic "pushover" results from FE models of the solid panel specimen (S2) and boundary frame using ABAQUS and from a strip model (Berman and Bruneau 2003) using SAP2000 (CSI 2002). Presented also in this figure is the experimental "backbone curve" (the peaks of each cycle) results from specimen S2 and the predicted strength for the frame (V_{yf}), panel (V_{yp}), and total ($V_{y.total}$) from equations presented in Vian and Bruneau (2005) and Vian et al. (2009). Results from FE analysis of the boundary frame were used, in conjunction with experimental and analytical results of the P and S2 specimen to quantify the contribution in terms of stiffness and strength of the infill panel.

Table 1. Comparison of Peak Results with Simplified Perforated Panel Models

Specimen	$K_{total}/K_{total.S2}$ (%)	$V_{y.total}/V_{y.total.S2}$ (%)	Observed K_{panel}[a] (kN/mm)	Observed K_{panel}[a] ($\%K_{panel.S2}$)	Predicted K_{perf}/K_{panel} w_{avg}/S_{diag} (%)	Predicted K_{perf}/K_{panel} w_{eff}/S_{diag} (%)	$V_{yp.perf}/V_{yp}$[b] Observed ($\%V_{yp.S2}$)	$V_{yp.perf}/V_{yp}$[b] Predicted Eq. (2)
P	88.5	84.6	73.0	78.1	86.3	82.2	66.7	67.0
CR	103.3	96.9	98.0	104.8	—	—	—	—
S2	—	—	93.5	—	—	—	—	—

[a]Assumes $K_{frame} \approx 42$ kN/mm as calculated from ABAQUS bare frame analysis (see Fig. 3).

[b]Assumes $V_{yf} \approx 1{,}200$ kN as calculated from ABAQUS bare frame analysis at $\Delta \approx 40$ mm.

Discussion of Results

Based on Fig. 3, both the SAP strip model and the ABAQUS shell element model captured the elastic stiffness of the specimen S2 well. The experimental stiffness was calculated as 136 kN/mm while the SAP and ABAQUS models had elastic stiffnesses of 115 and 150 kN/mm, respectively, underestimating and overestimating the experimental stiffness by 15 and 10%, respectively. The values for panel stiffness given by the expressions provided by Thorburn et al. (1983) for full tension field action, $K_{full.tfa}$, and partial tension field action, $K_{partial.tfa}$, are plotted in Fig. 3 for comparison. These models assume boundary frame members that are rigid against bending, and, therefore, significantly overestimate the panel stiffness as compared with the case considered here. The SAP and ABAQUS models both estimated the yield strength of the system reasonably well, as shown in Fig. 3. However, the SAP model underestimated the ultimate strength as compared with the ABAQUS and experimental results because the model did not account for cyclic strain hardening of the boundary frame elements.

Table 1 lists the stiffness and strength of each specimen, K_{total} and $V_{y.total}$, respectively, normalized by the corresponding value from the solid panel specimen S2, $K_{total.S2}$, and $V_{y.total.S2}$. The contributions of the infill panel to stiffness (i.e., K_{panel}) and strength (i.e., V_{yp}) are determined by subtracting the bare frame stiffness, K_{frame} (=42 kN/mm), and strength, V_{yf} (=1,200 kN at $\Delta=0$ mm) determined from the ABAQUS bare frame analysis results shown in Fig. 3. By this calculation, the perforated panel in specimen P had a stiffness of 78% that of the solid panel. This agreed well with the values predicted using the normalized average perforated strip width (w_{avg}/S_{diag}) presented in Vian and Bruneau (2005) and the normalized effective perforated strip width (w_{eff}/S_{diag}) presented in Vian et al. (2009) of 86 and 82%, respectively, which slightly underestimated the observed reduction in panel stiffness.

Fig. 4 presents an illustration of a typical perforated strip [Fig. 4(a)] and predicted versus observed panel stiffness reduction (w_{eff}/S_{diag}) as a function of the total length of perforations (N_rD) normalized by the total strip length ($H_{panel}/\sin\theta$) for constant N_r (solid lines) and constant S_{diag} (dashed lines) where N_r=number of perforation rows; H_{panel}=height of the panel, and D =perforation diameter [Fig. 4(b)]. The expression for the panel stiffness reduction derived from analysis of the typical perforated strip was evaluated for the as-built specimen P panel with a perforation ratio (D/S_{diag}) equal to 0.4714, which is noted and plotted with a bold line in Fig. 4(b). The intersection of D/S_{diag} =0.4714 with N_r=4, identified by a solid circle, represents the predicted stiffness reduction (82%). Plotted also is the calculated (based in part on experimental results) panel stiffness reduction 78%, which is in close agreement with the predicted value [note that the vertical axis in Fig. 4(b) is truncated, exaggerating the difference].

The perforated panel strength was determined to be approximately 500 kN at 2% drift after the frame contribution was subtracted from the total specimen P strength, reducing the strength of the perforated panel ($V_{yp.perf}$) to 67% of the solid panel (V_{yp} =750 kN). From Table 1, the stiffness (both total and panel only) and total strength of specimen CR displayed less than 5% difference from the values for specimen S2. This is satisfactory given that the intent was that the strength and stiffness of a specimen with corner cutouts would be effectively identical to those of the corresponding solid panel.

Observations and Design Considerations

LYS 165 versus A572 Infill Panel

Specimen P was fabricated using an infill panel with LYS165 steel exhibiting an elongation capacity of approximately 45%,

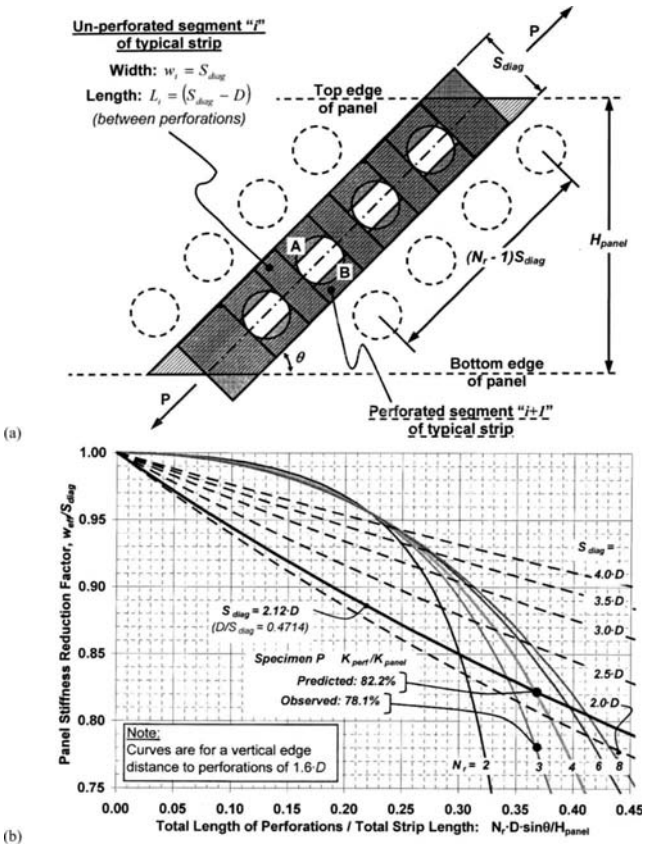

Fig. 4. Perforated panel: (a) typical diagonal strip; (b) predicted versus observed stiffness reductions

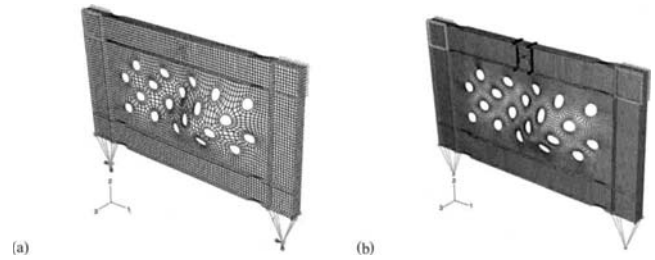

Fig. 5. FE model of specimen P with first panel buckling mode: (a) medium mesh; (b) fine mesh

greater than twice the minimum elongation required by the A36, A992, and A572 material specifications. Data from uniaxial strain gages located between perforation holes recorded specimen infill panel strains that correlated well with those of the ABAQUS model at their corresponding locations (Vian and Bruneau 2005). Nonetheless, an additional model with finer mesh was developed and used to investigate the localized distribution of panel stress and strain between perforations. Fig. 5 shows the medium and fine meshed FE model of specimen P and the first buckling mode of the infill panel from eigenvalue analysis. The fine mesh model was subjected to a monotonic pushover loading, producing maximum computed infill strains of 13% (approximately one-third of the maximum elongation of the tension tests) at locations adjacent to perforations when the drift reached the maximum value measured during testing.

Additionally, the fine mesh model of specimen P was reanalyzed using a different infill panel material to examine the effect of material properties on maximum strains adjacent to perforations. Infill panel properties were assigned using a cyclic stabilized backbone curve for A572 Grade 50 steel ["Steel A" from Kaufmann et al. (2001)]. The panel thickness was modified from the 2.6 mm tested, to 1.5 mm, such that the ultimate strength per unit panel width, $F_u \cdot t$, was approximately equal to the tested LYS165 panel. This thickness is 58% of the tested LYS165 panel, and 30% of the typical minimum available thickness for A572 plate: 5 mm (0.1875 in.).

A monotonic pushover displacement loading was applied to the revised model to investigate the strain concentrations around panel perforations. Fig. 6 shows the monotonic force versus displacement relationship for the LYS165 and A572 infill panels obtained from this analysis, compared with the specimen P experimental and analytical cyclic results. Maximum principal in-plane strains adjacent to the perforations reached 10% at a frame drift of 1.2%, equivalent to 49% of the drift reached by the LYS infill panel specimen when its maximum strain reached the same value of 10%. Pushed further, the higher strength infill panel reached a local maximum strain of 20%, at 1.8% drift, or 39% of the drift in the LYS panel reached at a similar strain of 20%. More extensive results are provided in Purba and Bruneau (2007). Note that 20% is roughly equal to the minimum elongation required by the ASTM A572 specification.

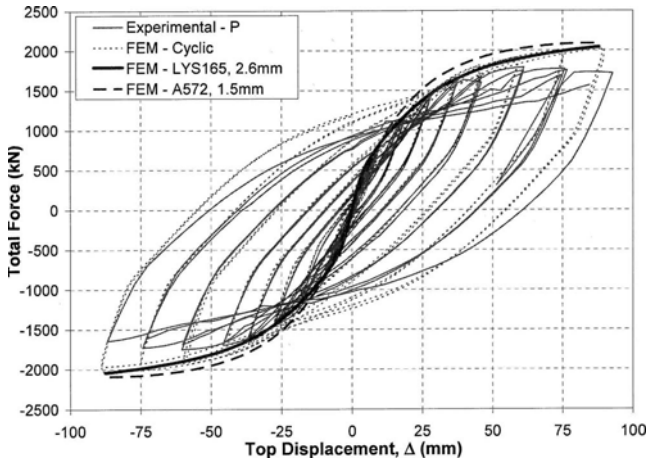

Fig. 6. Comparison of cyclic (experimental versus FEM) and monotonic (FEM with LYS165 and A572 infill) results

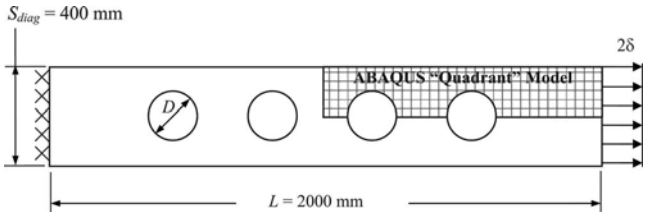

Fig. 7. Illustration of perforated strip geometry

The ductile behavior exhibited by the perforated infill panel specimen benefited from the panel being of low yield strength steel, LYS165. However, the above results show that similar adequate ductile performance would be obtained using common North American steel grades. Design guidelines are provided in the next section to ensure adequate ductility of perforated infill panels using A36 [F_y=36 ksi (248 MPa)] and A572 [F_y=50 ksi (345 MPa)] steel grades. Those design limits for SPSWs with perforated plates are based on minimum specified tensile properties (i.e., per the relevant ASTM material specification) for yield and ultimate strength, as well as minimum elongation. An investigation of panel strain behavior for a range of hole geometries also served to develop design recommendations for limiting perforation sizes to facilitate ductile response, as discussed in the subsequent section.

Design Considerations

The yield strength of a solid panel V_{yp} is calculated as

$$V_{yp} = \frac{1}{2} F_{yp} \cdot t \cdot W_{panel} \sin 2\alpha \quad (1)$$

where F_{yp}=panel yield strength; t=panel thickness; W_{panel}=panel width, and α=inclination of the tension field force with respect to the vertical. It had earlier been suggested that the perforated panel strength yield strength $V_{yp.perf}$ could be calculated by reducing the strength of a solid panel yield force V_{yp} with the same overall dimensions by use of the factor, $1-D/S_{diag}$, i.e.

$$V_{yp.perf} = \left(1 - \frac{D}{S_{diag}}\right) \cdot V_{yp} \quad (2)$$

To assess the validity of this concept, Purba and Bruneau (2007) investigated the behavior of individual perforated strips as a subelement of perforated SPSW using the finite element software ABAQUS/Standard. In this study, finite element analyses were performed for strips having a perforation diameter D ranging from 10 to 300 mm, corresponding to a perforation ratio D/S_{diag} varying from 0.025 to 0.75. An illustration of the perforated strip geometry and the region modeled using ABAQUS is presented in Fig. 7. Each strip was loaded using a monotonic

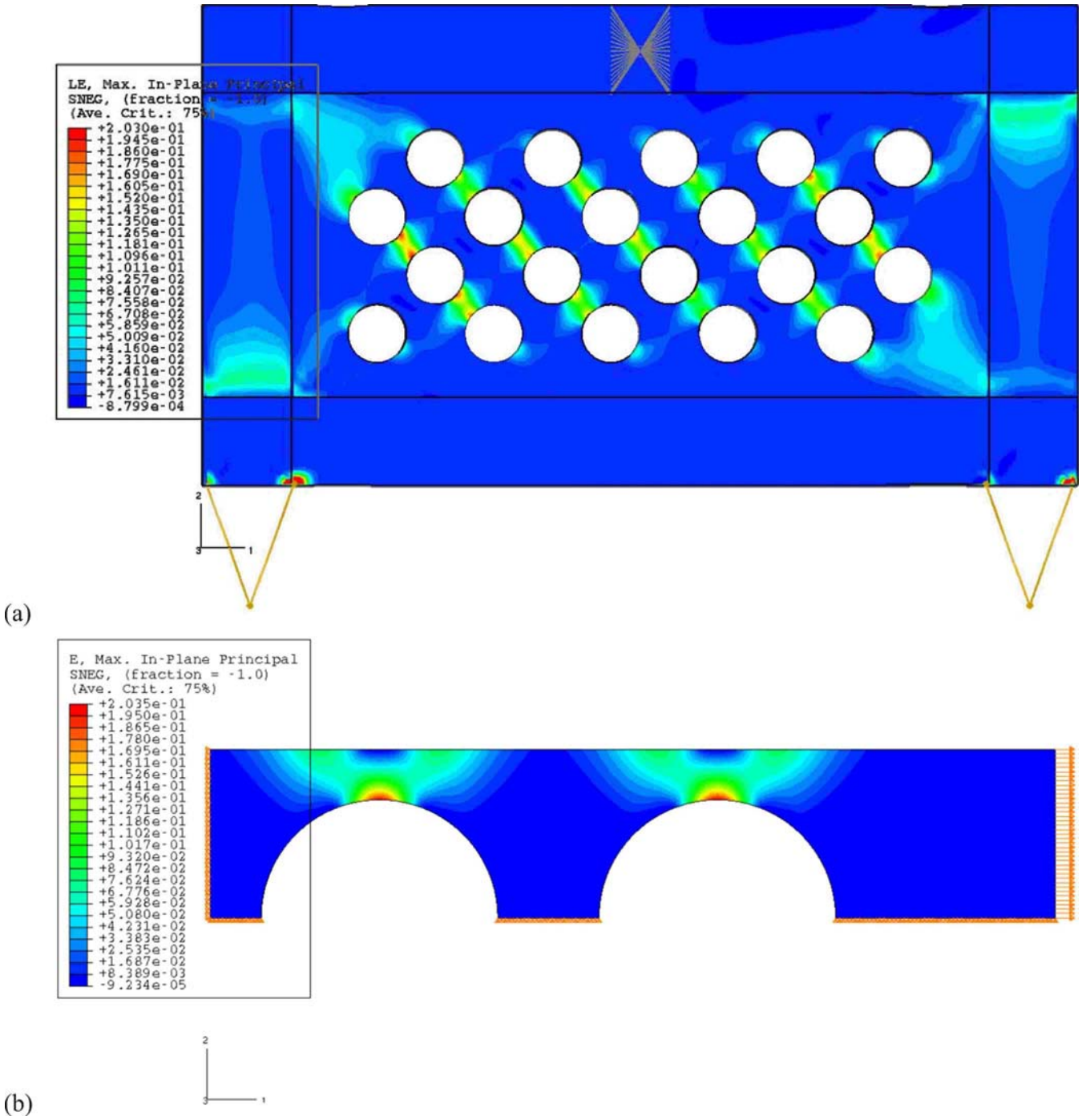

Fig. 8. Maximum in-plane principal strain from FE models: (a) panel; (b) strip

incremental displacement δ applied uniformly along the right edge up to a total displacement value of 50 mm, corresponding to a total uniform strip elongation, ε_{un} (=δ/L), of 5%. For each analysis (D/S_{diag} ratio), the total uniform strip elongation was recorded when a maximum principal local strain, ε_{max}, at a point in the strip reached a value of 1, 5, 10, 15, and 20%.

Additionally, finite element analyses of full SPSW were performed to investigate the relationship between perforation diameter and infill panel strain, to verify the accuracy of the individual strip model results, and to investigate the influence of the boundary element stiffness/rigidity on the stress and strain distribution in the panel. Similar to the strip model, FE analysis of the SPSW was performed with panel perforation diameters (D) of 50, 100, 150, 200, 250, and 300 mm. Fig. 8 illustrates typical maximum in-plane principal strain contours for the panel [Fig. 8(a)] and strip [Fig. 8(b)] FE models. Fig. 9 presents total uniform strip elongation (ε_{un}=δ/L) versus perforation ratio (D/S_{diag}) for maximum principal strain (ε_{max}) values of 1, 5, 10, 15, and 20% from analyses performed using the strip and panel models. For a given D/S_{diag} and ε_{max}, the total uniform strip elongation from the strip and panel models agree well. For example, for a D/S_{diag}=0.35 and ε_{max}=15%, a total uniform strip elongation of, approximately, 1.8 is observed in the strip and panel models. Although some differences are observed at the 20% monitoring strain, however, in all cases a less than 15% difference is observed and considered acceptable.

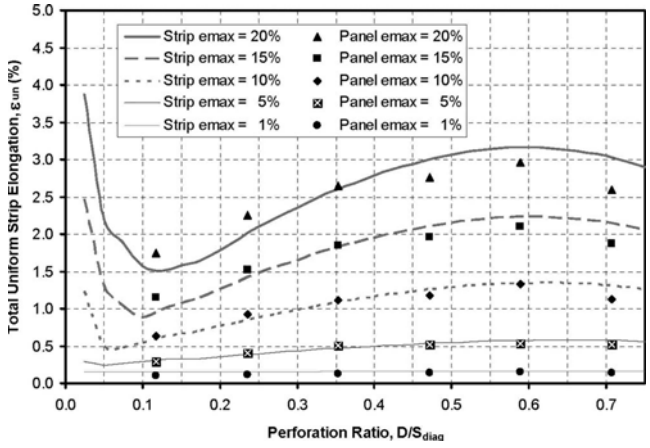

Fig. 9. Uniform distributed strip axial strain ε_{un} versus perforation ratio D/S_{diag}

Results of analyses performed with the full SPSW model were used to assess the applicability of Eq. (2) for SPSW panels having multiple perforations. For comparison purposes, a SPSW having a solid infill panel was also analyzed. For both the solid and perforated SPSW models, the infill panel strength was determined by subtracting the strength of the boundary frame determined from an additional analysis of the boundary frame alone. Fig. 10 presents infill plate strength ratios ($V_{yp.perf}/V_{yp}$) versus perforation ratios (D/S_{diag}) for frame drifts (γ) of 1, 2, 3, 4, and 5%. Additionally, the predicted value of Eq. (2) is also plotted in Fig. 10 (as a solid line) along with the results of a linear regression analysis performed on the FE data (as a dotted line). Based on the results presented in Fig. 10, an improved equation is proposed

$$\frac{V_{yp.perf}}{V_{yp}} = \left[1 - 0.7\frac{D}{S_{diag}}\right] \tag{3}$$

where the value of 0.7 is based on the results of the linear regression analysis.

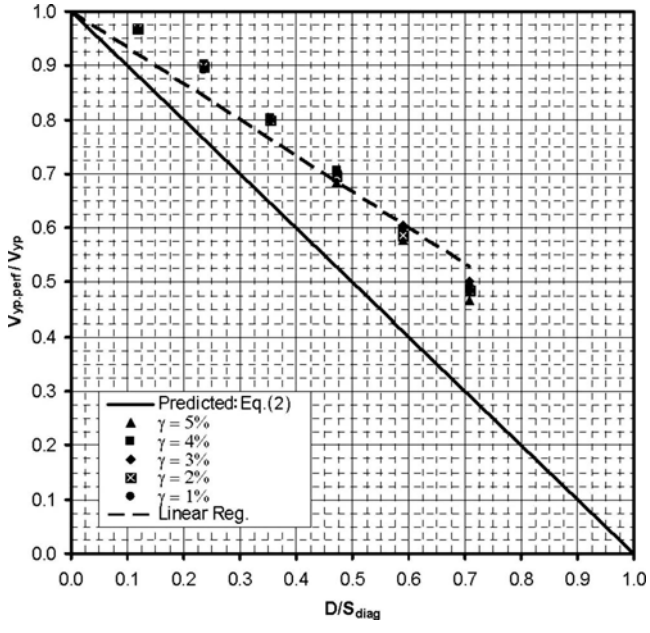

Fig. 10. Infill plate strength ratios ($V_{yp.perf}/V_{yp}$) versus perforation ratio (D/S_{diag})

The infill plate strength ratio ($V_{yp.perf}/V_{yp}$) was calculated for the specimen P panel ($D/S_{diag}=0.4714$) using Eq. (3) and agrees well with the experimentally observed value presented in Table 1.

Conclusions

The finite element analysis software package ABAQUS/Standard was used to perform nonlinear quasi-static monotonic and cyclic analyses of models representing the tested specimens described in Vian et al. (2009). Good agreement in overall behavior between the test results and the monotonic and cyclic analyses were observed, suggesting that the modeling assumptions utilized in this case are appropriate for modeling other SPSW problems.

The results were compared with the simpler strip models and manual calculations, which were used in the design of the specimens and development of the experimental displacement loading history. It is observed that simpler strip models also provide a reasonable estimate of displacement and strength at initial yield. Good agreement with observed experimental results was given by the proposed design equation for calculating the relative strength and stiffness of perforated panels.

A specially detailed perforated panel SPSW specimen exhibited ductile behavior during testing. This result, combined with that of an FE analytical study, demonstrated that this system is a viable alternative to a solid panel SPSW, without the need for stiffeners around the perforations as required by current seismic design specifications (AISC 2005). This system could allow utility access through the panel and is also recommended for use in SPSW applications for which, if the minimum available plate thickness is too large, the effective strength of the solid panel must be reduced to minimize the force demand (from capacity design) on the surrounding frame.

It is recommended that future seismic design specifications follow the proposed guidelines suggested for perforation layout to ensure ductile performance of this system during a seismic event. It is estimated that SPSW system drifts during the design earthquake should be typically less than 1.5% and all systems tested as part of this project performed satisfactorily up to a 2% drift.

The cutout reinforced corner system also performed well during testing and appears to be an effective solution for SPSW implementation and allows for the passage of utilities at panel corners near to the columns.

Acknowledgments

This work was supported in part by the Earthquake Engineering Research Centers Program of the National Science Foundation under Award No. ECC-9701471 to the Multidisciplinary Center for Earthquake Engineering Research. The assistance of Dr. Gordon Warn during manuscript preparation is also appreciated. However, any opinions, findings, conclusions, and recommendations presented in this paper are those of the writers and do not necessarily reflect the views of the sponsors.

References

AISC. (2005). "Seismic provisions for structural steel buildings." *ANSI/AISC 341-05*, American Institute of Steel Construction, Inc., Chicago, Ill.

Berman, J. W., and Bruneau, M. (2003). "Plastic analysis and design of

steel plate shear walls." *J. Struct. Eng.*, 129(11), 1148–1156.

Computers and Structures Inc. (CSI). (2002). *SAP2000: Analysis reference manual*, Ver. 8.0, Berkeley, Calif.

Dafalias, Y. F., and Popov, E. P. (1976). "Plastic internal variables formalism of cyclic plasticity." *J. Appl. Mech.*, 43, 645–651.

Driver, R. G., Kulak, G. L., Kennedy, D. J. L., and Elwi, A. E. (1997). "Seismic behavior of steel plate shear walls." *Structural Engineering Rep. No.*, *215*, Dept. of Civil and Environmental Engineering, Univ. of Alberta.

Hibbitt, Karlsson, and Sorenson, Inc. (HKS). (2002). *ABAQUS/standard users' manual*, Ver. 6.3, Hibbitt, Karlsson, and Sorenson, Inc., Pawtucket, R.I.

Hodge, P. G., Jr. (1957). "Discussion of Prager's (1956) 'A new method of analyzing stress and strains in work-hardening solids.'" *J. Appl. Mech.*, 23, 482–484.

Kaufmann, E. J., Metrovich, B., and Pense, A. W. (2001). "Characterization of cyclic inelastic strain behavior on properties of A572 Gr. 50 and A913 Gr. 50 rolled sections." *ATLSS Rep. No. 01-13*, National Center for Engineering Research on Advanced Technology for Large Structural Systems, Lehigh Univ., Bethlehem, Pa.

Krieg, R. D. (1975). "A practical two-surface plasticity theory." *J. Appl. Mech.*, 42, 641–646.

Lemaitre, J., and Chaboche, J.-L. (1990). *Mechanics of solid materials*, Cambridge University Press, Cambridge, U.K.

Purba, R., and Bruneau, M. (2007). "Design recommendations for perforated steel plate shear walls." *Tech. Rep.No. MCEER-07–0011*, Multidisciplinary Center for Earthquake Engineering Research, State Univ. of New York at Buffalo, Buffalo, N.Y.

Thorburn, L. J., and Kulak, G. L., and Montgomery, C. J. (1983). "Analysis of steel plate shear walls." *Structural Engineering Rep. No.*, *107*, Dept. of Civil Engineering, Univ. of Alberta, Edmonton, Alberta, Canada.

Vian, D., and Bruneau, M. (2005). "Steel plate shear walls for seismic design and retrofit of building structures." *Tech. Rep. No. MCEER-05–0010*, Multidisciplinary Center for Earthquake Engineering Research, State Univ. of New York at Buffalo, Buffalo, N.Y.

Vian, D., Bruneau, M., Tsai, K. C., and Lin, Y.-C. (2009). "Special perforated steel plate shear walls with reduced beam section anchor beams. I: Experimental investigation." *J. Struct. Eng.* 135(3).